Available online at www.sciencedirect.com

jmr&t Journal of Materials Research and Technology

journal homepage: www.elsevier.com/locate/jmrt

Original Article

Synthesis and optical properties investigation of blue-excitable red-emitting $K_2Bi(PO_4)$ (MoO_4):Pr^{3+} powders

Julija Grigorjevaite, Arturas Katelnikovas *

Institute of Chemistry, Faculty of Chemistry and Geosciences, Vilnius University, Naugarduko 24, LT–03225, Vilnius, Lithuania

ARTICLE INFO

Article history:
Received 8 October 2020
Accepted 18 November 2020
Available online 24 November 2020

Keywords:
Red phosphor
Thermal quenching
Color coordinates
Inorganic materials
Luminescence
Cross-relaxation
Trivalent praseodymium

ABSTRACT

A series of $K_2Bi(PO_4)$ (MoO_4) samples doped with 0.5%–50% Pr^{3+} was synthesized by a solid state synthesis method. The crystal phase was monitored by powder X-ray diffraction (XRD) and morphological characteristics were investigated by scanning electron microscopy (SEM). The luminescence properties: photoluminescence excitation and emission spectra, thermal quenching, and fluorescence lifetime values of Pr^{3+}- doped samples were evaluated. The samples showed orange-red luminescence under near-UV excitation. It turned out that the profile of Pr^{3+} emission spectra is concentration and temperature dependent. Concentration quenching was observed in samples with higher than 1% Pr^{3+} concentration. Moreover, the calculated color coordinates showed good thermal stability in the 77–500 K temperature range. Based on the obtained results it can be concluded that prepared samples can be used in luminescent security pigments.

1. Introduction

The rare earth element praseodymium, incorporated into the inorganic host matrices, shows efficient luminescence only in its trivalent state [1]. The trivalent praseodymium ion exhibits the emission in very broad spectrum range, i.e., from deep UV through the visible to near infrared [2]. Inorganic materials, doped with Pr^{3+} ions, can exhibit both intraconfigurational (4f ↔ 4f) and interconfigurational (5d ↔ 4f) transitions; therefore, they find numerous applications in important technological fields. For instance, trivalent praseodymium doped materials become popular for applications as scintillators due to the allowed 5d → 4f transitions of Pr^{3+}, also it can provide photoluminescence decay time even faster than Ce^{3+} doped materials. However, this transition strongly depends on the host matrix, because the lowest 5d level can relax by multiphoton emission to the closest in energy 4f levels [3]. The narrow emission lines originating from the 4f → 4f transitions of Pr^{3+} doped materials find applications in lighting, display, and security industry [4–6].

The direct transitions from ^3P_J ($J = 0, 1, 2$) or $^1D_2$ excited levels to the ground states (^3H_J) results in sharp lines in the Pr^{3+} emission spectra. Besides, in some host matrixes, the

* *Corresponding author.*
E-mail address: arturas.katelnikovas@chf.vu.lt (A. Katelnikovas).
https://doi.org/10.1016/j.jmrt.2020.11.054

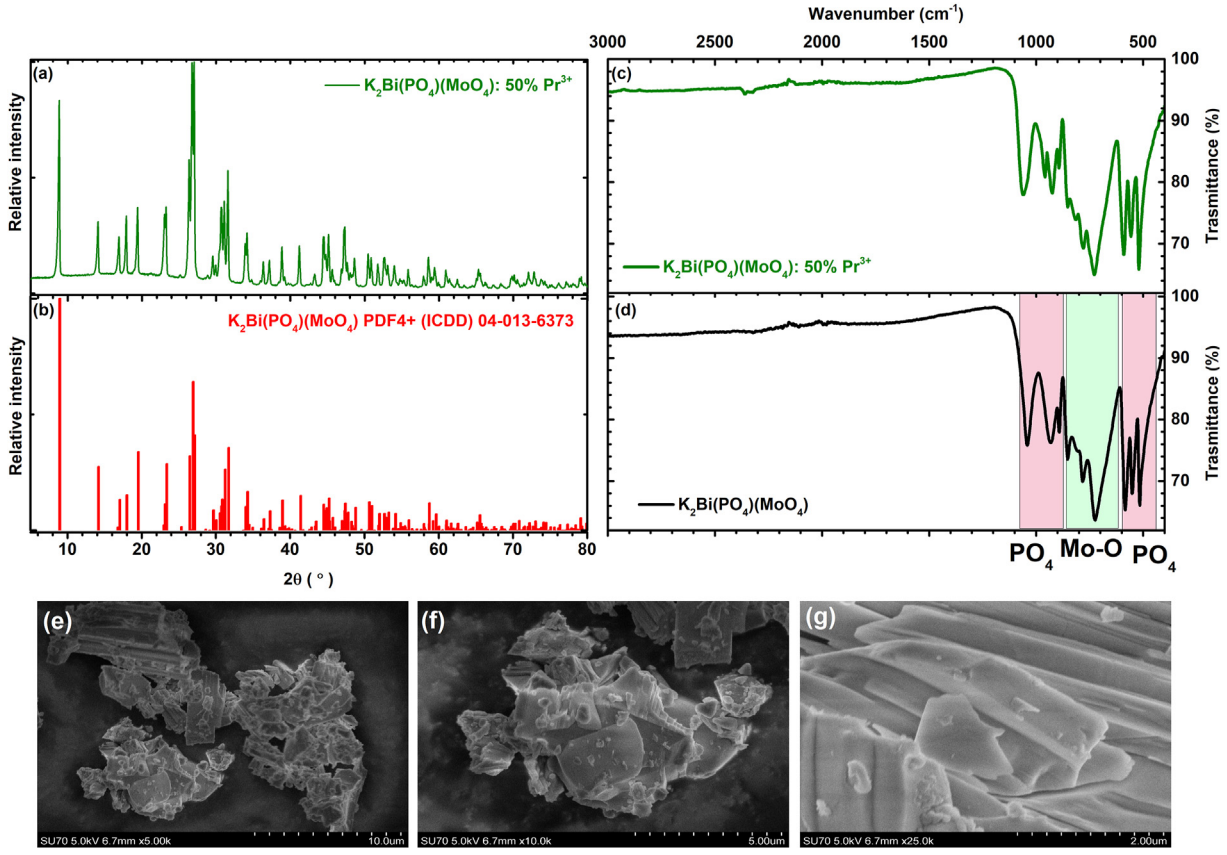

Fig. 1 – (a) Powder XRD patterns of $K_2Bi(PO_4)$ (MoO_4):50%Pr^{3+}, (b) XRD reference pattern of $K_2Bi(PO_4)$ (MoO_4); (c) FTIR spectra of $K_2Bi(PO_4)$ (MoO_4):50% Pr^{3+} and (d) undoped $K_2Bi(PO_4)$ (MoO_4); (e), (f), and (g) high resolution SEM images of $K_2Bi(PO_4)$ (MoO_4):0.5% Pr^{3+} powders under different magnification.

energy migration from ^3P_J to $^1D_2$ levels can be observed yielding exclusively only red emission [7,8]. In the studied host matrix, namely, $K_2Bi(PO_4)$ (MoO_4), only intraconfigurational (4f → 4f) transitions were observed, but in other hosts, especially with low covalency and weak crystal fields, broad emission bands can be observed due to interconfigurational (5d → 4f) transitions, for instance, YPO_4:Pr^{3+}, YBO_3:Pr^{3+}, KYF_4:Pr^{3+}, etc. [9,10]. Also, cross-relaxation processes are very common in inorganic materials doped with trivalent praseodymium ions and this process is responsible for the emission quenching, especially as a function of dopant concentration [11]. The cross-relaxation process can be directly measured by examining the fluorescence decay after the pulsed excitation.

For the aforementioned reasons, Pr^{3+} doped $K_2Bi(PO_4)$ (MoO_4) synthesis and optical measurements were performed. As we mentioned before, the luminescence properties of rare-earth ions are determined by their environment in the host lattice. In most cases, molybdate based compounds are used as luminescent ion hosts in order to obtain a well-defined emission properties [12].

In this research, the $K_2Bi(PO_4)$ (MoO_4):Pr^{3+} phosphors were prepared by a solid state reaction method at relatively low temperature (873.15 K). The optical properties of synthesized samples were consistently studied as a function of Pr^{3+} concentration and temperature. The given data will include XRD and SEM measurements, reflection, excitation, emission spectra, PL decay curves, luminous efficacies at room temperature; and emission spectra, PL decay curves, as well as CIE 1931 color coordinates in 77–500 K temperature interval.

2. Methods

The synthesis of the pure and Pr^{3+} doped $K_2Bi(PO_4)$ (MoO_4) was performed according to Eq. (1).

$$K_2CO_3 + NH_4H_2PO_4 + MoO_3 + Bi_2O_3/Pr_6O_{11} \rightarrow K_2(Bi,Pr)\ (PO_4)\ (MoO_4) + \text{gaseous products} \quad (1)$$

The stoichiometric amounts of high purity raw materials K_2CO_3 (99+% Acros Organics), $NH_4H_2PO_4$ (99% Reachem Slovakia), MoO_3 (99+ Acros Organics), Bi_2O_3 (99.9% Acros Organics) and Pr_6O_{11} (99.9% Aldrich) were weighed and mixed in an agate mortar using acetone as a grinding media. The blended powder was transferred to the porcelain crucible, capped and annealed at 873.15 K for 10 h. The calcination procedure was repeated another two times and samples were reground after each step. Finally, after the third annealing step, samples were cooled down to the room temperature by switching of the furnace. In order to measure the structural and optical properties of the phosphors, the samples were ground into the fine powders. The Pr^{3+} concentration in the

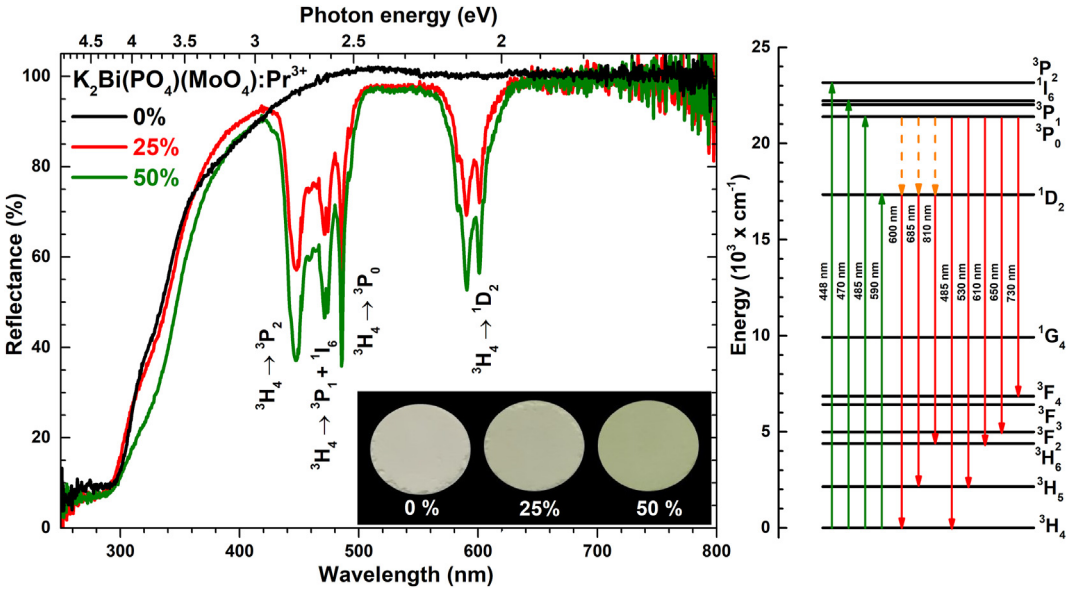

Fig. 2 – Reflection spectra of $K_2Bi(PO_4)(MoO_4)$ and $K_2Bi(PO_4)(MoO_4)$ doped with 25% and 50% Pr^{3+} (the left hand side), and simplified energy level diagram of Pr^{3+} ions showing the main 4f-4f transitions of the Pr^{3+} ion (the right hand side). Inset shows a digital photo of powder colour under daylight depending on Pr^{3+} concentration.

final compounds was 0%, 0.5%, 1%, 2.5%, 5%, 10%, 15%, 25% and 50%. The attempt to synthesize 75% Pr^{3+} and fully Pr^{3+} substituted compound ($K_2Pr(PO_4)(MoO_4)$), unfortunately, was not successful. It should also be noted that Pr^{4+} ions in a mixed valence Pr_6O_{11} oxide ($4PrO_2 \cdot Pr_2O_3$) during the annealing step got reduced to Pr^{3+} accompanied with release of oxygen gas. The simplified equation for this process could be written as $Pr_6O_{11} \rightarrow 3Pr_2O_3 + O_2$. Similar observations of PrO_2 oxide loosing oxygen even at annealing under air was reported by Chatzichristodoulou et al. [13,14] and Kuru [15].

The powder XRD patterns were collected on a Rigaku MiniFlexII diffractometer working in a Bragg–Brentano focusing geometry. The scanning speed and step width was 5°/min and 0.02°, respectively. SEM images were taken by a FE-SEM Hitachi SU-70. IR measurements were performed on a Bruker Alpha ATR FTIR spectrometer. The reflection, excitation and emission spectra, thermal quenching (TQ) were recorded on the modular Edinburgh Instruments FLS980 spectrometer.

The particular settings are given in detail in supporting information file (see Table S1 to Table S4).

3. Results and discussion

3.1. *Structural analysis*

The crystal structure of $K_2Bi(PO_4)(MoO_4)$ was first reported by I. Zatovsky and co-workers [16] in 2006. The paper reveals that $K_2Bi(PO_4)(MoO_4)$ adopts an orthorhombic crystal structure with a space group of Ibca (#73). The crystal structure is constructed by PO_4 and MoO_4 tetrahedra and eight-coordinated K^+ and Bi^{3+}/Pr^{3+} polyhedrons. Due to equal ionic charge and similar ionic radii, we expected that Bi^{3+} (1.17 Å for CN = 8) ions were substituted by Pr^{3+} (1.13 Å for CN = 8) ions [17,18]. The orthorhombic $K_2Bi(PO_4)(MoO_4)$ crystal structure was also extensively studied by many authors previously [18,19]. The powder XRD pattern of 50% Pr^{3+} doped compound is presented in Fig. 1a and $K_2Bi(PO_4)(MoO_4)$ (PDF4+ (ICDD) 04-013-6373) reference pattern is presented in Fig. 1b. The given results indicate that incorporation of Pr^{3+} up to 50% yields single phase compounds.

We have also performed the Le Bail fit of the obtained XRD patterns in order to investigate the lattice parameters changes upon Pr^{3+} concentration increase. The obtained results are given in Fig. S1. Even though the atomic radii of Bi^{3+} and Pr^{3+} ions are very close (the difference being just 3.5%) it was recently shown that even smaller ionic radii yield changes in unit cell parameters [20]. We have expected that with increase of Pr^{3+} concentration unit cell parameters would decrease, since Pr^{3+} ions are slightly smaller than Bi^{3+}. However, the opposite phenomenon was observed and all unit cell parameters increased. On the other hand, it should also be emphasized that the total change in the unit cell parameters is extremely small, just around few tenths of percent. Such behavior is rather unusual and requires further detailed research but it was also recently observed by Jiang et al. where larger Ba^{2+} ions were replaced by smaller Pb^{2+} ions in $CaBa_{1-x}Pb_xZn_2Ga_2O_7$ and expansion of the unit cell occurred [21].

The IR spectra of samples doped with 50% and 0% Pr^{3+} ions are depicted in Fig. 1c and d, respectively. The given IR spectra are virtually identical despite Bi^{3+}/Pr^{3+} ratio and are composed of few absorptions bands in the range of 400–1100 cm^{-1}. Three sharp absorption bands in the range of 650–450 cm^{-1} can be attributed to the PO_4 bending vibrations. Strong absorption bands at 950 cm^{-1} and 1050 cm^{-1} can be ascribed as symmetric and asymmetric vibrations of PO_4 tetrahedrons. Due to Mo–O stretching vibration in MoO_4 tetrahedrons, strong absorption band can be seen in the range of 900–700 cm^{-1} [18]. SEM images were taken and are depicted in

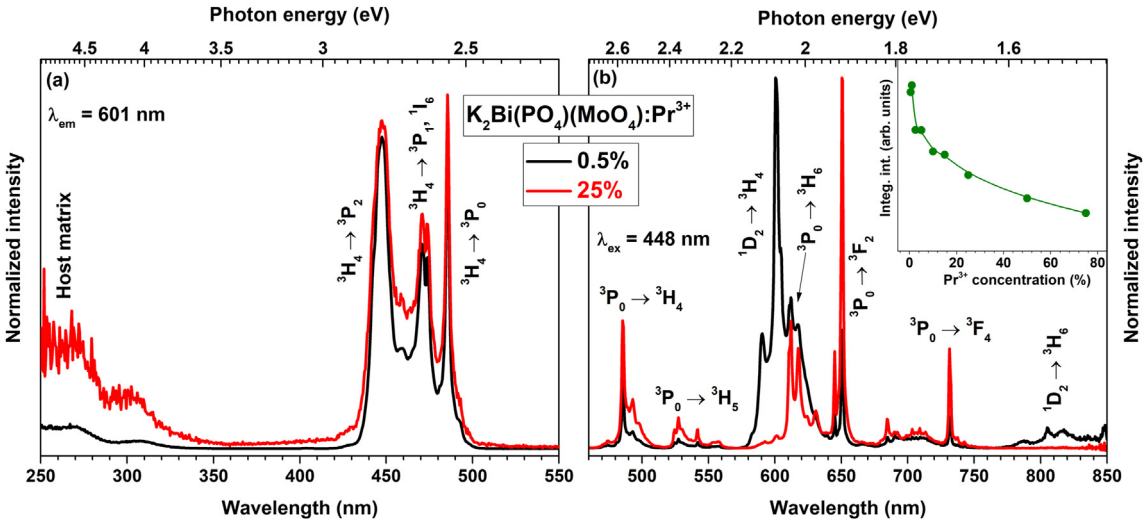

Fig. 3 – (a) Excitation (λ_{em} = 601 nm) and (b) emission (λ_{ex} = 448 nm) spectra of $K_2Bi(PO_4)$ (MoO_4) doped with 0.5% and 25% Pr^{3+}. Inset graph shows emission (λ_{ex} = 448 nm) integral intensity as a function of Pr^{3+} concentration.

Fig. 1e-g for the morphology features investigation of $K_2Bi(PO_4)$ (MoO_4):0.5%Pr^{3+} phosphor powder. The powder particles are formed from a rod-like small crystallites. No significant changes in crystallite size and shape were observed by changing Pr^{3+} concentration.

3.2. *Photoluminescence studies*

The body color of undoped sample is white, although all samples doped with Pr^{3+} ions were greenish due to absorption lines in the blue and red spectral region. As the concentration increases, the greenish powder color intensifies (see Fig. 2). This was confirmed by reflection spectra (see Fig. 2). The absorption lines in the blue spectral region is assigned to the $^3H_4 \rightarrow {}^3P_2$ (ca. 448 nm), $^3H_4 \rightarrow {}^3P_1 + {}^1I_6$ (ca. 472 nm) and $^3H_4 \rightarrow {}^3P_0$ (ca. 486 nm) transitions. The set of absorption lines in the red spectral region is assigned to the $^3H_4 \rightarrow {}^1D_2$ (ca. 597 nm) transition. Besides, the reflectance in the longer wavelength region is close to unity what shows high brilliance of the synthesized phosphor powders. The simplified energy level diagram of Pr^{3+} ions is given on the right hand side of Fig. 2 with the most common 4f-4f transitions marked [22]. It was clearly seen that various transitions from the excited ^3P_J (J = 0, 1, 2) and $^1D_2$ states can occur in Pr^{3+} containing systems, among them the $^3P_0 \rightarrow {}^3F_2$ and the $^1D_2 \rightarrow {}^3H_4$ transitions, which are associated with intense orange-red emissions at ca. 600 nm. Red-orange luminescence emission is frequent feature in MoO_4^{2-} matrixes doped with Pr^{3+} ions due to low energy MoO_4^{2-} charge transfer state [23,24]. It is also evident that the UV absorption band of Pr^{3+} doped samples is slightly shifted to the longer wavelengths (lower energies) and this feature can be attributed to the Pr^{3+} $4f^2 \rightarrow 4f^15d^1$ absorption.

The excitation spectra of Pr^{3+} ions in $K_2Bi(PO_4)$ (MoO_4) host are shown in Fig. 3a. These spectra consist of several sharp lines in the region from 430 nm to 500 nm corresponding to the $^3H_4 \rightarrow {}^3P_2$, (ca. 450 nm), $^3H_4 \rightarrow {}^3P_1$, $^1I_6$ (ca. 470 nm), and $^3H_4 \rightarrow {}^3P_0$ (ca. 480 nm) transitions and the broad band in the region from 250 nm to 300 nm [22]. The origin of this broad band is most likely due to a host matrix absorption. The emission spectra of 0.5% and 25% of Pr^{3+} doped $K_2Bi(PO_4)$ (MoO_4) specimens are depicted in Fig. 3b. The emission spectra contain six sets of lines that originate from $^3P_0 \rightarrow {}^3H_4$ (ca. 486 nm), $^3P_0 \rightarrow {}^3H_5$ (ca. 529 nm), $^1D_2 \rightarrow {}^3H_4$ (ca. 590–630 nm), $^3P_0 \rightarrow {}^3H_6$ (ca. 615 nm), $^3P_0 \rightarrow {}^3F_2$ (ca. 650 nm), $^3P_0 \rightarrow {}^3F_4$ (ca. 735 nm), and $^1D_2 \rightarrow {}^3H_6$ (ca. 808 nm) transitions [22]. The maximum emission intensity was achieved if phosphors were doped with 1% Pr^{3+} (λ_{ex} = 448 nm). Further increase of Pr^{3+} concentration leads to emission intensity decrease (see Fig. 3b inset) due to concentration quenching. The emission spectra are very similar for the different Pr^{3+} concentrations, although $^1D_2 \rightarrow {}^3H_4$ transition shows a strong concentration quenching. This appearance is often observed in the emission spectra of Pr^{3+} ions [25–27] and can be clarified as concentration quenching due to cross-relaxation between adjacent Pr^{3+} ions [26]. These relaxation mechanisms can be written as $^1D_2 + {}^3H_4 \rightarrow {}^1G_4 + {}^3F_4$ and $^1D_2 + {}^3H_4 \rightarrow {}^3F_4 + {}^1G_4$ [28].

Fig. 4 depicts the PL decay curves of the $^1D_2 \rightarrow {}^3H_4$ (ca. 601 nm) transition of $K_2Bi(PO_4)$ (MoO_4):Pr^{3+} samples as a function of Pr^{3+} concentration when samples were excited at 448 nm ($^3H_4 \rightarrow {}^3P_2$ transition) and emission monitored at 601 nm. The PL decay curves become steeper with increasing Pr^{3+} concentration and this feature indicates that PL lifetime values get lower. The inset of the Fig. 4 shows τ_{eff} values for the different Pr^{3+} concentrations. In order to calculate the effective PL lifetime values, the following equation was used (Eq. (2)) [29]:

$$\tau_{eff} = \frac{\int_0^{\infty} I(t)t\ dt}{\int_0^{\infty} I(t)\ dt} \quad (2)$$

Here $I(t)$ is PL intensity at a given time t. The effective PL lifetime values are tabulated in Table S5 and were found to vary from 66 μs to ca. 3 μs for the 0.5% and 25% dopant concentration, respectively. This feature is likely caused by a higher probability of cross-relaxation processes [11]. This

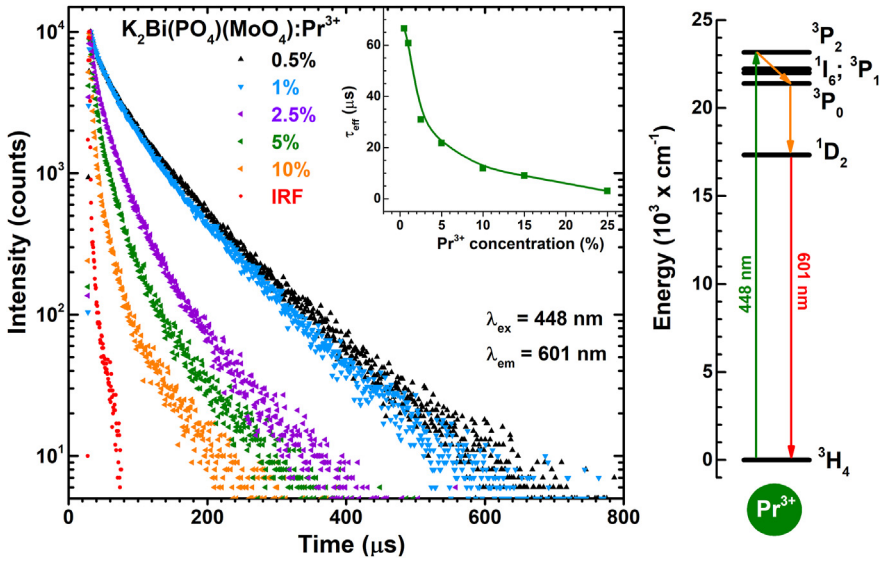

Fig. 4 – PL decay curves (λ_{ex} = 448 nm, λ_{em} = 601 nm) of $K_2Bi(PO_4)(MoO_4):Pr^{3+}$ as a function of Pr^{3+} concentration (the left hand side). Inset shows average τ_{eff} values as a function of Pr^{3+} concentration; graphic on the right hand side shows a fragment of Pr^{3+} energy levels with $^3H_4 \rightarrow {}^3P_2$ and $^1D_2 \rightarrow {}^3H_4$ transitions.

drastic decrease of the effective PL lifetime values, when Pr^{3+} concentration increases, points to the strong quenching of the emission from $^1D_2$ level as was also observed in concentration dependent emission spectra depicted in Fig. 3.

The temperature dependent emission and excitation spectra were recorded in the range of 77 K–500 K in order to evaluate phosphors performance at elevated temperatures. Temperature dependent excitation and emission spectra of 1% doped $K_2Bi(PO_4)$ (MoO_4) sample are shown in Fig. 5a and b, respectively. Sample doped with 1% Pr^{3+} was chosen for the temperature dependent measurements since it shows the highest emission intensity. The inset of the Fig. 5b shows the normalized temperature dependent integral intensity of the sample. The emission intensity is stable in the range of 77–300 K and only above 350 K starts to sharply decrease. The emission intensity decrease at elevated temperatures is caused by thermal quenching.

At 77 K temperature the lines in emission spectrum are well resolved and very sharp. However, when temperature was increased to 500 K the peaks became so much broadened that they are not distinguishable anymore. From the temperature dependent emission integral data, the $TQ_{1/2}$ value was determined. $TQ_{1/2}$ value shows the temperature at which the phosphor loses half of its efficiency. The thermal quenching activation energy (E_A) can be also determined from the temperature dependent integrated emission spectra employing the Fermi-Dirac model [30–32] (see Eq. (3)).

$$\frac{I(T)}{I_0} = \frac{1}{1 + Be^{-E_A/kT}} \tag{3}$$

Here $I(T)$ and I_0 are temperature dependent emission integral and the highest value of emission integral, respectively. B is the quenching frequency factor. E_A is activation energy, k is Boltzmann constant ($8.617342 \cdot 10^{-5}$ eV/K) [33], and T is

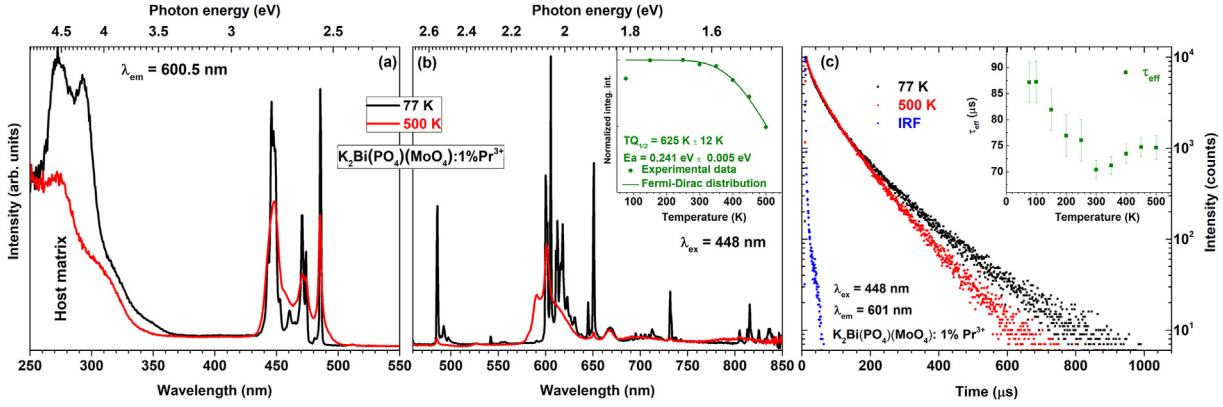

Fig. 5 – (a) Temperature dependent excitation (λ_{em} = 600.5 nm) and (b) emission (λ_{ex} = 448 nm) spectra of $K_2Bi(PO_4)$ (MoO_4) doped with 1% Pr^{3+}, (b inset) shows calculation of $TQ_{1/2}$ and E_a values for the sample doped with 1% Pr^{3+}, (c) shows PL decay curves (λ_{ex} = 488 nm, λ_{em} = 601 nm) of $K_2Bi(PO_4)$ $(MoO_4):Pr^{3+}$ as a function of temperature (IRF stands for the Instrument Response Function), (c inset) shows τ_{eff} values as a function of temperature.

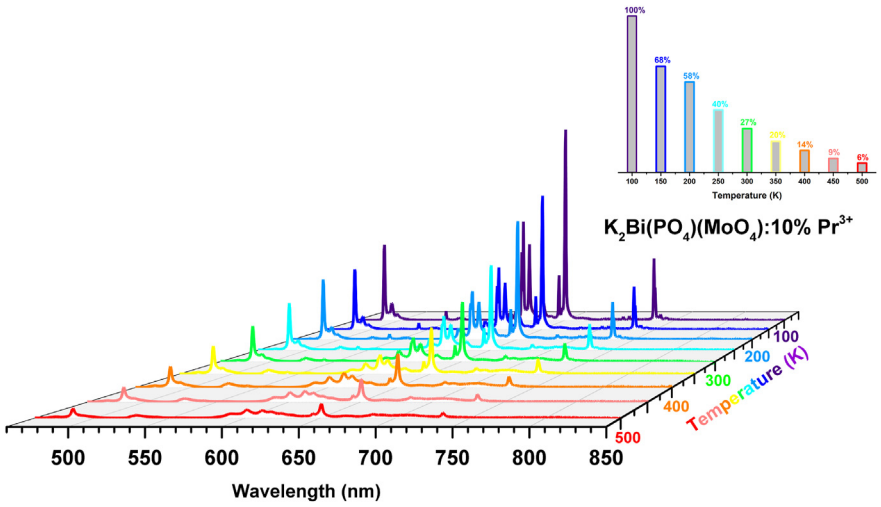

Fig. 6 – Temperature dependent emission (λ_{ex} = 448 nm) spectra of $K_2Bi(PO_4)(MoO_4)$ doped with 10% Pr^{3+} ranging from 100 K to 500 K with inset of the integrated emission intensity at different temperatures.

temperature in K. A slight modification of Eq. (3) yields Eq. (4), which gives the $TQ_{1/2}$ values:

$$TQ_{1/2} = \frac{-E_A}{k \times \ln(1/B)} \quad (4)$$

After calculation using Eqs (3) and (4) it was revealed that $TQ_{1/2} = 625\ K \pm 12\ K$ and $E_A = 0.241\ eV \pm 0.005\ eV$ for the 1% Pr^{3+} doped sample. In this host matrix, $TQ_{1/2}$ value is very high, if compared, for instance, $Y_2Mo_4O_{15}$: 0.5% Pr^{3+} phosphors where $TQ_{1/2}$ is equal to 400 K ± 7 K and E_A is 0.19 eV ± 0.02 eV [34].

The temperature dependent photoluminescence decay curves of $K_2Bi(PO_4)$ (MoO_4) sample doped with 1% Pr^{3+} were also recorded and depicted in Fig. 5c. It was found out that temperature has no significant effect on the shape of PL decay curves; therefore, in this case, the PL decay curves recorded at 77 K and 500 K are only shown. From every temperature dependent PL decay curve, the effective PL lifetime values were calculated and plotted in the inset of Fig. 5c. The effective PL lifetime values (λ_{ex} = 448 nm, λ_{em} = 601 nm) of $K_2Bi(PO_4)$ (MoO_4) phosphors doped with 1% Pr^{3+} varied from ca. 87 μs to ca.75 μs in the temperature range from 77 K to 500 K (see Table S6). The effective PL lifetime values slightly decrease from ca. 87 μs to ca. 70 μs when temperature is increased from 77 to 300 K, and then again increase from ca. 70 μs to ca. 75 μs with further temperature increase to 500 K. However, it should also be noted, that the estimated PL values in the temperature range of 300–500 K fluctuate within the margin of the calculation error.

The similar thermal quenching behavior was observed for the sample doped with 10% Pr^{3+} ions (see Fig. 6). The inset of Fig. 6 represents the integrated emission intensity at different temperatures which obviously decreases when the temperature increases. At first the intensity decrease massively from 100% to 58% when the temperature is increased from 100 K to 200 K, but then intensity slightly decrease from 58% to 6% when temperature is increased from 200 K to 500 K. Low (100 K) temperature emission spectra are dominated by $^3P_0 \rightarrow {}^3H_4$, $^1D_2 \rightarrow {}^3H_4$, $^3P_0 \rightarrow {}^3H_6$ and $^3P_0 \rightarrow {}^3F_4$ transitions. However, when temperature was increased to 500 K all transitions from $^3P_0$ and $^1D_2$ almost disappeared. This feature is expected, because of cross-relaxation and $^1D_2$ level is absolutely vanished in non-radiative pathway [34], and only emission from $^3P_0 \rightarrow {}^3H_4$, $^3H_6$, and $^3F_4$ transitions at 590, 601 and 740 nm are seen in the spectra at 500 K temperature.

The energy gap between $^3P_0$ and $^1G_4$ levels is 11469 cm^{-1} and it is almost the same as energy gap separating the $^1G_4$ and $^3H_4$ ground state (9921 cm^{-1}) [35]. Concurrently, energy gap between $^1D_2$ and $^3F_4$ is 10479.6 cm^{-1} and between $^3H_4$ and $^1G_4$ is 9921 cm^{-1} [11]. According to this, the energy mismatch for $^3P_0$ transitions is 1547 cm^{-1} while for cross-relaxation $^1D_2$ transitions mismatch is 558 cm^{-1}. As a result of the smaller energy mismatch for the cross-relaxation process for the ground state, cross-relaxation is more active for the $^1D_2$ versus the $^3P_0$ level. The energy difference (Δ*E*) between the involved transitions are given in Table 1 [36].

3.3. *Photometric*

Color coordinates of $K_2Bi(PO_4)$ (MoO_4):Pr^{3+} as a function of Pr^{3+} are shown in Fig. 7a. The color coordinates shift towards lower *x* and larger *y* values with increasing Pr^{3+} concentration. All prepared samples were orange-red emitting and the calculated precise CIE 1931 color coordinates of samples are tabulated in Table S7. The temperature dependent color coordinates of 1% and 10% doped samples were also calculated and are depicted in Fig. 7b and c, respectively. The precise temperature dependent color coordinates are given in

Table 1 – Energies of transitions involved in cross-relaxation process between Pr^{3+} ions. D and A stand for donor and acceptor, respectively.

Pr^{3+} (D)		Pr^{3+} (A)	
Transition	Δ*E* (cm^{-1})	Transition	Δ*E* (cm^{-1})
$^1G_4 \rightarrow {}^3H_4$	9921	$^1D_2 \rightarrow {}^3F_4$	10480
$^1G_4 \rightarrow {}^3P_0$	11469	$^3H_4 \rightarrow {}^1G_4$	9921

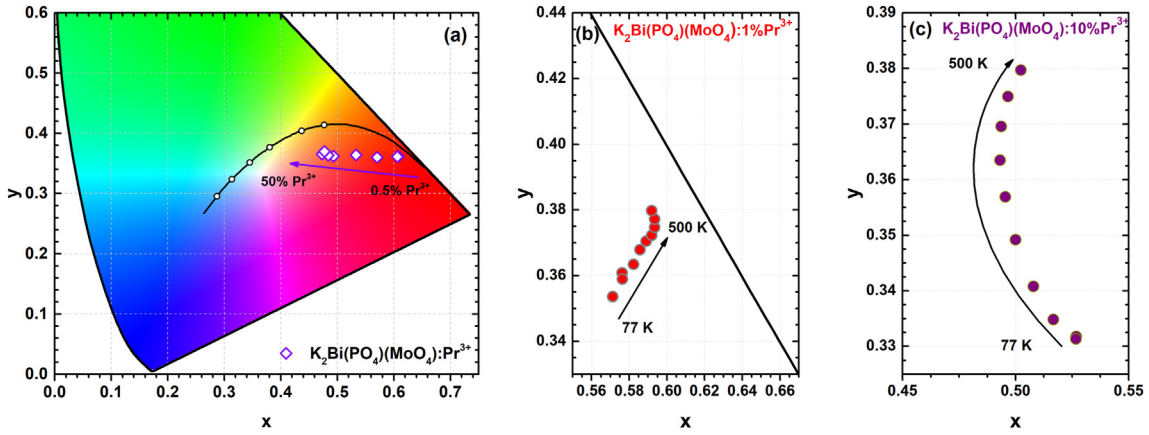

Fig. 7 – CIE 1931 color space diagram and color coordinates of $K_2Bi(PO_4)$ (MoO_4):Pr^{3+} phosphors as a function of Pr^{3+} concentration (a), temperature dependent color coordinates of 1% Pr^{3+} (b), and 10% Pr^{3+} (c) doped samples.

Table S8. Color coordinates slightly shifted towards the edge of the CIE 1931 diagram with increasing temperature.

The external quantum efficiencies (*EQE*) of the synthesized phosphors under 448 nm (blue light) were also determined using integrating sphere method. Samples doped with 0.5%, 1%, 2.5%, and 5% Pr^{3+} possessed *EQE* values of 5.5%, 7.1%, 3.8%, and 2.2%, respectively. Unfortunately, it was not possible to measure *EQE* values for the samples doped with higher amounts of Pr^{3+} ions, because the emission was already too weak.

4. Conclusions

Single phase $K_2Bi(PO_4)$ (MoO_4) doped with Pr^{3+} phosphors were synthesized by simple solid state reaction method. Samples were doped up to 50%, the single phase with 75% and 100% Pr^{3+} was not obtained. The body color of synthesized phosphors was greenish and show orange-red emission if phosphors were excited with blue (448 nm) radiation. The highest emission intensity was obtained for the sample doped with 1% of Pr^{3+}, the further increase of concentration leads to emission decrease due to concentration quenching. The $^1D_2 \rightarrow {}^3H_4$ (ca. 590–630 nm) transition of Pr^{3+} ions in the given host matrix shows an exceptionally strong concentration quenching. The color coordinates of the phosphors show good thermal stability. It was determined that the sample with the most intense emission would lose half of its efficiency only at 625 K temperature; therefore, it could be applicable in fields where high operating temperatures are required. These features show that synthesized materials can be used in display and security pigments industry.

Funding

This research was funded by a grant (No. S-MIP-17-48) from the Research Council of Lithuania.

Author contributions

conceptualization, A.K.; investigation, J.G.; writing – original draft preparation, J.G.; writing – review and editing, A.K.; visualization J.G.; funding acquisition. A.K.

Declaration of Competing Interest

The authors declare that they have no known competing financial interests or personal relationships that could have appeared to influence the work reported in this paper.

Acknowledgment

The authors gratefully thank Rokas Vargalis (Vilnius University) for taking SEM images.

Appendix A. Supplementary data

Supplementary data to this article can be found online at https://doi.org/10.1016/j.jmrt.2020.11.054.

REFERENCES

[1] Rodnyi PA, Mishin AN, Potapov AS. Luminescence of trivalent praseodymium in oxides and fluorides. Optic Spectrosc 2002;93:714–21. https://doi.org/10.1134/1.1523992.
[2] Liang YJ, Liu F, Chen YF, Wang XL, Sun KN, Pan ZW. Red/near-infrared/short-wave infrared multi-band persistent luminescence in Pr^{3+}-doped persistent phosphors. Dalton Trans 2017;46:11149–53. https://doi.org/10.1039/c7dt02271a.
[3] Zhuravleva M, Novoselov A, Yoshikawa A, Pejchal J, Nikl M, Fukuda T. Crystal growth and scintillation properties of Pr-doped $YAlO_3$. Opt Mater 2007;30:171–3. https://doi.org/10.1016/j.optmat.2006.11.057.

[4] Xu B, Liu J, Song C, Luo H, Jie Peng Y, Yu XB. Synthesis and tunable luminescent properties of red phosphor $Li_{1-m}AgmLa_{0.99-n}Y_nPr_{0.01}(MoO_4)_2$ with blue excitation for white LEDs. J Am Ceram Soc 2012;95:250–6. https://doi.org/10.1111/j.1551-2916.2011.04764.x.

[5] Guan Y, Tsuboi T, Huang YL, Huang W. Broadband infrared emission of Pr^{3+}-doped $BaGd_2(MoO_4)_4$ for optical amplifier. J Appl Phys 2014;115:213104. https://doi.org/10.1063/1.4881116.

[6] Srivastava AM. Aspects of Pr^{3+} luminescence in solids. J Lumin 2016;169:445–9. https://doi.org/10.1016/j.jlumin.2015.07.001.

[7] Boutinaud P, Pinel E, Oubaha M, Mahiou R, Cavalli E, Bettinelli M. Making red emitting phosphors with Pr^{3+}. Opt Mater 2006;28:9–13. https://doi.org/10.1016/j.optmat.2004.09.027.

[8] Pinel E, Boutinaud P, Mahiou R. Using a structural criterion for the selection of red-emitting oxide-based compounds containing Pr^{3+}. J Alloys Compd 2004;374:165–8. https://doi.org/10.1016/j.jallcom.2003.11.084.

[9] Broxtermann M, den Engelsen D, Fern GR, Harris P, Ireland TG, Justel T, et al. Cathodoluminescence and photoluminescence of $YPO_4:Pr^{3+}$, $Y_2SiO_5:Pr^{3+}$, YBO_3: Pr^{3+}, and $YPO_4:Bi^{3+}$. ECS J Solid State Sci 2017;6:R47–52. https://doi.org/10.1149/2.0051704jss.

[10] Kristianpoller N, Weiss D, Khaidukov N, Makhov V, Chen R. Thermoluminescence of some Pr^{3+} doped fluoride crystals. Radiat Meas 2008;43:245–8. https://doi.org/10.1016/j.radmeas.2007.11.001.

[11] Naccache R, Vetrone F, Speghini A, Bettinelli M, Capobianco JA. Cross-relaxation and upconversion processes in Pr^{3+} singly doped and Pr^{3+}/Yb^{3+} codoped nanocrystalline $Gd_3Ga_5O_{12}$: the sensitizer/activator relationship. J Phys Chem C 2008;112:7750–6. https://doi.org/10.1021/jp711494d.

[12] Benoit G, Veronique J, Arnaud A, Alain G. Luminescence properties of tungstates and molybdates phosphors: illustration on $ALn(MO_4)_2$ compounds (A = alikaline cation, Ln = lanthanides, M = W, Mo). Solid State Sci 2011;13:460–7. https://doi.org/10.1016/j.solidstatesciences.2010.12.013.

[13] Chatzichristodoulou C, Hendriksen PV, Hagen A. Defect chemistry and thermomechanical properties of $Ce_{0.8}Pr_xTb_{0.2-x}O_{2-\delta}$. J Electrochem Soc 2010;157:B299–307. https://doi.org/10.1149/1.3270475.

[14] Chatzichristodoulou C, Hendriksen PV. Oxygen nonstoichiometry and defect chemistry modeling of $Ce_{0.8}Pr_{0.2}O_{2-\delta}$. J Electrochem Soc 2010;157:B481–9. https://doi.org/10.1149/1.3288241.

[15] Kuru Y, Bishop SR, Kim JJ, Yildiz B, Tuller HL. Chemomechanical properties and microstructural stability of nanocrystalline Pr-doped ceria: an in situ X-ray diffraction investigation. Solid State Ionics 2011;193:1–4. https://doi.org/10.1016/j.ssi.2011.04.012.

[16] Zatovsky IV, Terebilenko KV, Slobodyanik NS, Baumer VN, Shishkin OV. $K_2Bi(PO_4)(WO_4)$ with a layered anionic substructure. Acta Crystallogr E 2006;62:I193–5. https://doi.org/10.1107/S1600536806033265.

[17] Shannon RD. Revised effective ionic radii and systematic studies of interatomic distances in halides and chalcogenides. Acta Crystallogr 1976;A32:751–67. https://doi.org/10.1107/S0567739476001551.

[18] Zatovsky IV, Terebilenko KV, Slobodyanik NS, Baumer VN, Shishkin OV. Synthesis, characterization and crystal structure of $K_2Bi(PO_4)(MoO_4)$. J Solid State Chem 2006;179:3550–5. https://doi.org/10.1016/j.jssc.2006.07.027.

[19] Grigorjevaite J, Ezerskyte E, Minderyte A, Stanionyte S, Juskenas R, Sakirzanovas S, et al. Optical properties of red-emitting $Rb_2Bi(PO_4)(MoO_4):Eu^{3+}$ powders and ceramics with high quantum efficiency for white LEDs. Materials 2019;12:3275. https://doi.org/10.3390/ma12193275.

[20] Liu XL, Song Z, Kong YW, Wang SX, Zhang SY, Xia ZG, et al. Effects of full-range Eu concentration on $Sr_{2-2x}Eu_{2x}Si_5N_8$ phosphors: a deep-red emission and luminescent thermal quenching. J Alloys Compd 2019;770:1069–77. https://doi.org/10.1016/j.jallcom.2018.08.236.

[21] Jiang PF, Neuefeind JC, Avdeev M, Huang QZ, Yue MF, Yang XY, et al. Unprecedented lattice volume expansion on doping stereochemically active Pb^{2+} into uniaxially strained structure of $CaBa_{1-x}Pb_xZn_2Ga_2O_7$. Nat Commun 2020;11:1303. https://doi.org/10.1038/s41467-020-14759-2.

[22] Carnall WT, Crosswhite H, Crosswhite HM. Energy level structure and transition probabilities in the spectra of the trivalent lanthanides in LaF_3. Argonne National Laboratory Report; 1977.

[23] Chun FJ, Li W, Zhang BB, Deng W, Chu X, Su H, et al. Visible and near-infrared luminescent properties of Pr^{3+} doped strontium molybdate thin films by a facile polymer-assisted deposition process. J Colloid Interface Sci 2018;531:181–8. https://doi.org/10.1016/j.jcis.2018.07.040.

[24] Qiao XB, Tsuboi T. Emission from Mo-O charge-transfer state and Yb^{3+} emission in Eu^{3+}-doped and nondoped molybdates under UV excitation. J Am Ceram Soc 2017;100:1440–51. https://doi.org/10.1111/jace.14679.

[25] Donega CD, Lambaerts H, Meijerink A, Blasse G. The vibronic spectroscopy of Pr^{3+} in YocI and LaocI. J Phys Chem Solid 1993;54:873–81. https://doi.org/10.1016/0022-3697(93)90212-A.

[26] Dornauf H, Heber J. Concentration-dependent fluorescence-quenching in $La_{1-x}Pr_xP_5O_{14}$. J Lumin 1980;22:1–16. https://doi.org/10.1016/0022-2313(80)90040-X.

[27] Donega CDM, Ellens A, Meijerink A, Blasse G. Concentration enhancement of the vibronic transitions of the Pr^{3+} ion. J Phys Chem Solid 1993;54:293–300. https://doi.org/10.1016/0022-3697(93)90261-O.

[28] Del Longo L, Ferrari M, Zanghellini E, Bettinelli M, Capobianco JA, Montagna M, et al. Optical spectroscopy of zinc borate glass activated by Pr^{3+} ions. J Non-Cryst Solids 1998;231:178–88. https://doi.org/10.1016/S0022-3093(98)00409-8.

[29] Lahoz F, Martin IR, Mendez-Ramos J, Nunez P. Dopant distribution in a Tm^{3+}-Yb^{3+} codoped silica based glass ceramic: an infrared-laser induced upconversion study. J Chem Phys 2004;120:6180–90. https://doi.org/10.1063/1.1652016.

[30] Baur F, Glocker F, Justel T. Photoluminescence and energy transfer rates and efficiencies in Eu^{3+} activated $Tb_2Mo_3O_{12}$. J Mater Chem C 2015;3:2054–64. https://doi.org/10.1039/c4tc02588a.

[31] Ueda J, Dorenbos P, Bos AJJ, Meijerink A, Tanabe S. Insight into the thermal quenching mechanism for $Y_3Al_5O_{12}:Ce^{3+}$ through thermo luminescence excitation spectroscopy. J Phys Chem C 2015;119:25003–8. https://doi.org/10.1021/acs.jpcc.5b08828.

[32] Muller M, Fischer S, Justel T. Luminescence and energy transfer of co-doped $Sr_5MgLa_2(BO_3)_6:Ce^{3+},Mn^{2+}$. RSC Adv 2015;5:67979–87. https://doi.org/10.1039/c5ra12951f.

[33] Lide DR, Haynes WM, editors. CRC handbook of chemistry and physics. 90th ed. Boca Raton, FL: CRC Press/Taylor and Francis; 2010 (CD-ROM Version 2010).

[34] Mackeviciute I, Linkeviciute A, Katelnikovas A. Synthesis and optical properties of $Y_2Mo_4O_{15}$ doped by Pr^{3+}. J Lumin 2017;190:525–30. https://doi.org/10.1016/j.jlumin.2017.06.014.

[35] Donega CD, Meijerink A, Blasse G. Nonradiative relaxation processes of the Pr^{3+} ion in solids. J Phys Chem Solid 1995;56:673–85. https://doi.org/10.1016/0022-3697(94)00183-9.

[36] Carnall WT, Fields PR, Rajnak K. Electronic energy levels in the trivalent lanthanide aquo ions. I Pr^{3+}, Nd^{3+}, Pm^{3+}, Sm^{3+}, Dy^{3+}, Ho^{3+}, Er^{3+} and Tm^{3+}. J Chem Phys 1968;49:4425–42. https://doi.org/10.1063/1.1669893.